Enhanced subsurface response for marine CSEM surveying

Frank A. Maaø[1] and Anh Kiet Nguyen[2]

ABSTRACT

One of the main challenges of using marine controlled-source electromagnetic (CSEM) sounding for hydrocarbon detection has been a relatively low-resolution and restricted depth penetration. In addition, the use of CSEM in shallow waters has been perceived as particularly difficult. A new, robust method for enhancing marine CSEM subsurface response is particularly useful in shallow waters. The method is designed to reduce acquisition imprints and attenuate the dominant primary airwave contribution. Synthetic examples show that it is possible to detect thin, deeply buried 3D resistive bodies in a shallow-water environment with a complex resistivity structure. The results highlight the importance of a sufficient signal-to-noise ratio.

INTRODUCTION

CSEM was originally used as a general tool for investigation of the marine subsurface (Chave and Cox, 1982). In the early attempts to use marine CSEM measurements for hydrocarbon exploration, an application called seabed logging (SBL), it was considered to be a deepwater exploration technology (Eidesmo et al., 2002). This was caused mainly by the reduced relative response from thin resistive layers in a shallow-water environment. For an introduction to CSEM, we refer to MacGregor and Sinha (2000), Ellingsrud et al. (2002), and Constable and Srnka (2007).

Recent investigations, however, reveal that sufficient subsurface response for detection of thin resistive layers is usually present in shallow-water environments also. Mittet (2008) shows that anomalous responses can be seen in very shallow waters (40 m), and Weiss (2007) concludes that transient measurements in 100 m of water can detect targets at 2-km burial depth.

Several methods have been proposed to enhance the subsurface response in a shallow-water environment. Among these are up-down separation (Amundsen et al., 2006), usage of azimuth data (Løseth and Amundsen, 2007), and the application of spatial deconvolution methods (van den Berg et al., 2008). These methods often require very high measurement accuracy. To extract information that constitutes a small fraction of the total signal, the subtraction process must be done with a very high degree of accuracy. It is therefore important to find enhancement methods for the subsurface response that are robust against acquisition and other uncertainties present in the measurements. We now present a new technique for enhancing the CSEM subsurface response that shows particularly large potential in a shallow-water environment and is robust against many acquisition uncertainties.

THEORY

The significance of any measured physical quantity, F^{obs}, can be accessed by comparing its deviation from some hypothetical value, F^{synth}, with its uncertainty, ΔF^{obs}. This is often expressed in terms of an ℓ^2-norm misfit function

$$\varepsilon = \frac{|F^{\mathrm{obs}} - F^{\mathrm{synth}}|^2}{|\Delta F^{\mathrm{obs}}|^2} \equiv \frac{|F^{\mathrm{obs}} - F^{\mathrm{synth}}|^2}{\alpha^2 |F^{\mathrm{obs}}|^2 + |n_F|^2}. \tag{1}$$

Here, ΔF^{obs} is split into two parts — one multiplicative part, $\alpha|F^{\mathrm{obs}}|$, and one additive part, $|n_F|$. The multiplicative uncertainty typically arises from uncertainties in the acquisition parameters (positions, orientations, etc.) when the uncertainty of a measurement is proportional to the measured value. For example, assume an uncertainty in the estimated receiver rotation angle $\Delta\theta$. Then the uncertainty in the measured vector field $F = F_0 \cos(\theta)$ is $\Delta F \approx F_0 \sin(\theta)\Delta\theta$, which is proportional to the amplitude of the field. The additive uncertainty, on the other hand, is independent of the amplitude of the measured signal, typically denoted as noise, which may depend on acquisition parameters such as frequency and position, $n_F(f,x)$. Such noise can be caused by instrumentation or by any external uncontrolled signals. For marine electromagnetic measurements, external noise sources can be caused by natural radiation, swell, and seawater currents. A typical requirement for having a significant deviation between quantities F^{obs} and F^{synth} is $\varepsilon > 1$. A significant deviation between two scenarios then depends both on the sensitivity of F toward

changes in the subsurface and on measurement precision.

Often, sensitivity can be enhanced by using derived quantities. However, derived quantities often involve an increase in uncertainty, and this may reduce the overall benefit. Consider, however, the electric field measured at two frequencies but on the same channel and with the same source position and orientation. We define the frequency-differenced field as

$$F(\omega) = E(\omega + \Delta\omega) - E(\omega). \qquad (2)$$

For many acquisition parameters, the multiplicative uncertainty for this field will be proportional to $F(\omega)$ and *not* $E(\omega)$. Mathematically, the uncertainty for a derived quantity is $\Delta F = \sqrt{\Sigma_i (dF/d\beta_i)^2 (\Delta\beta_i)^2}$, where β_i labels independent measured quantities, and $\Delta\beta_i$ labels their uncertainties. As an example, consider that the uncertainty of the x-component of F caused uncertainty in the receiver orientation, θ. The uncertainty in F resulting from the uncertainty $\Delta\theta$ becomes $\Delta F_x(\theta)^2 = (E_y(\omega + \Delta\omega) - E_y(\omega))\Delta\theta^2$, which is proportional to F. However, if we combine data from two receivers (for instance, if we would like to calculate spatial gradients, Andreis and MacGregor,

2008), i and j, the corresponding uncertainty would be $\Delta F_x(\theta_i, \theta_j)^2 = E_y(\omega)^2 \Delta\theta_i^2 + E_y(\omega)^2 \Delta\theta_j^2$, which is proportional to E.

The frequency-differenced field can also be interpreted in terms of the transient impulse response because

$$F(\omega) = E(\omega + \Delta\omega) - E(\omega) \approx \Delta\omega \partial_\omega E(\omega)$$

$$= \Delta\omega \int_0^\infty dt(it)E(t)e^{i\omega t}. \qquad (3)$$

Thus, it emphasizes late-coming "events" in the signal and can show a high degree of subsurface sensitivity. Furthermore, in shallow water, the frequency-differenced field strongly attenuates early events as the primary airwave. In the following, we will show some basic results from 3D modeling and a synthetic case study with inversion. Based on this, we will discuss the potential for this method.

MODELING EXAMPLE

A synthetic inline electric field was created using 3D modeling (Maaø, 2007). Other 3D modeling techniques may be found in Commer and Newman (2008) and in Plessix and Mulder (2008).

The resistivity model consists of 100 m of water (0.3 Ωm), a homogenous background formation (2 Ωm), and a thin (50-m) resistive body with an elliptical shape (50 Ωm) at 4-km burial depth. The resistive body has semimajor and semiminor axes of 6 km and 4 km in the x- and y- directions, respectively (Figure 1).

The relevance of the increased sensitivity of frequency-differenced fields should be accessed through the misfit function (equation 1). For simplicity, the multiplicative uncertainty is set to 5% ($\alpha = 0.05$), and the additive uncertainty $|n_F|$ is assumed to be a constant noise level. The square root of the misfit function is shown for various situations in Figure 2. We refer to this quantity as the weighted sensitivity. The noise levels used in these examples are $|n_F| = 1.0 \times 10^{-14}$ and 1.0×10^{-15} V/Am^2. Whereas the inline electric field shows little response to the target and is not much affected by the noise level, the frequency-differenced field shows a much higher weighted sensitivity. At low noise levels, the weighted sensitivities can be larger by more than an order of magnitude.
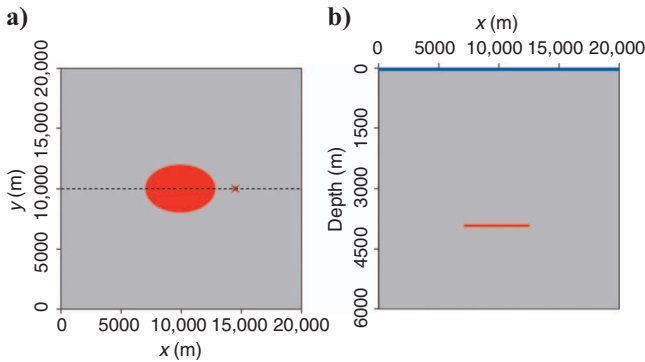

Figure 1. A model used in the numerical example study consists of 100 m of water, a homogenous background formation, and a 50-m-thick resistive body. The resistivities are 0.3, 2.0, and 50 Ωm, respectively. The semimajor and semiminor axes of the elliptical resistivity body are 6 km and 4 km with burial depth of 4 km. (a) Horizontal cross section at target depth. Black dashed line indicates the source towline. The receiver position is marked with an x. Sources and receiver are in the water layer. (b) Vertical cross section.

INVERSION EXAMPLE

The misfit function defined in equation 1 was implemented in 2.5D inversion (Hansen and Mittet, 2009). Another implementation of 2.5D inversion may be found in Abubakar et al. (2008). Two inversion schemes were implemented, one with only the inline electric field in the misfit and one in which the frequency-differenced field (equation 2) was added into the misfit in addition to the conventional inline electric field. We test the performance of the misfit functions using synthetic data from the 3D model shown in Figure 3. The model consists of a highly resistive basement (150 Ωm) with large lateral variation in burial depth and large uplifts (two salt bodies) into the nearby overburden. The model also includes two layers of relatively high resistivity of 6 Ωm and 10 Ωm just below the target. The target
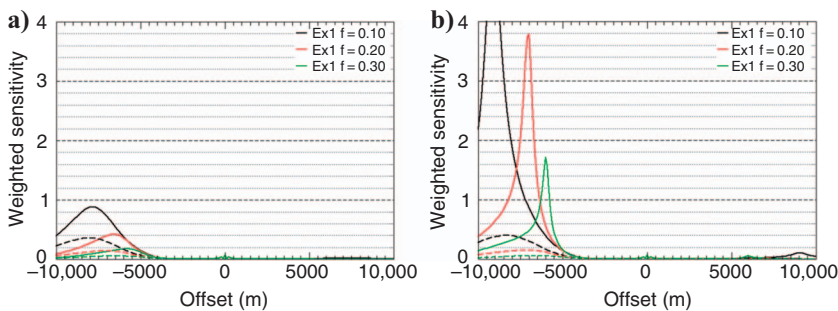

Figure 2. Numerical results for weighted sensitivity for different noise levels as a function of source-receiver offset for three frequencies: 0.1 Hz (black), 0.2 Hz (red), and 0.3 Hz (green). Dashed lines refer to inline electric fields, and solid lines refer to frequency-differenced fields. (a) Noise level $n_F = 1.0 \times 10^{-14}$ V/Am^2. (b) Noise level $n_F = 1.0 \times 10^{-15}$ V/Am^2. The difference in frequencies was set to 0.1 Hz in the frequency-differenced fields.

(100 Ωm) is 100 m thick and has a nearly elliptical shape at a 45° angle to the towline. It is approximately 2 km wide × 4 km long under the towline. The target depth is 3 km, and the resistivity of the overburden is 2 Ωm. The water depth (0.3 Ωm) is 100 m. The towline cross section of the model is shown in Figure 3. The numerical grids were $50 \times 100 \times 100$ m³ in the 3D modeling and 200×50 m² in the 2.5D inversion.

In the inversion, the four layers below the target are inverted as homogeneous resistivity blocks, whereas the rest of the model is inverted grid cell by grid cell. We use the background model as the starting model. Weak smoothness regularization is applied to stabilize the inversion. The frequencies selected for the inversion were 0.1, 0.2, and 0.3 Hz, with equal amplitudes, $\alpha = 0.05$ and $|n_F| = 3.0 \times 10^{-15}$. White noise with amplitude 3.0×10^{-15} V/Am² is added to the data prior to the inversion.

Figure 4 shows the inverted models (4a) after adding the frequency-differenced field into the misfit function and Figure 4b, using only the conventional inline electric field. We see in Figure 4 that the 2.5D inversion with the frequency-differenced field inserts a resistivity anomaly at the correct depth. The anomaly was shifted slightly laterally because of the 3D shape of the reservoir that is not accounted for in a 2.5D inversion scheme. Thus, the lateral position of the inverted resistive target is more in agreement with the center of the 3D target than with the position of the target at the given cross section.

In contrast to this, 2.5D inversion using only the electric field is not able to find any resistivity anomaly. We also notice that when the frequency-differenced field is added to the misfit function, it provides much better resistivity of the constrained layers compared with the true model. In both cases, the average misfit for the inverted model is only 0.001, which corresponds to an average data error of 3%.

DISCUSSION

To minimize uncertainty, the proposed method assumes data acquired on the same channel with signals emitted at the same source position and orientation. The latter can be obtained by emitting signals at two or more frequencies simultaneously. The only multiplicative uncertainty left, which is proportional to the original frequency-dependent data, is therefore due to the measurement of the source current and the calibration of the signal at the given frequencies. Note that any known systematic error in the frequency components can be compensated for and will not generate additional uncertainty. It should be noted that selecting frequencies that are too close together will yield differences which are more disposed to end up at the noise level or below. On the other hand, selecting frequencies too far apart will result in differences that are completely dominated by the low-frequency component. As shown in Mittet (2008), the scattered fields caused by the presence of thin resistive layers are usually larger in shallow waters than in deeper waters. Thus, aiming at methods to completely remove the sea-surface interaction also means reducing the magnitude of the scattered field. For sufficiently small or deep structures, the scattered field may therefore end up below the effective noise floor. In the examples presented, the scattered field of the frequency-differenced field has been of similar magnitude to the scattered field of the original field.

In the final stage of the reviewing process of this paper, Chen and Alumbaugh (2009) published a similar frequency-differencing method for mitigating the airwave in shallow water. Note, however, that the main aspect of our results is the reduction in the multiplicative uncertainties that enhances the significance of the measurements. The primary airwave attenuation is merely a positive side effect.

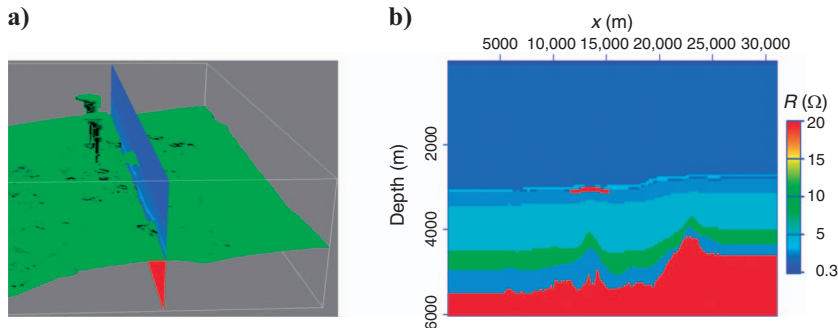**a)**   **b)**

Figure 3. (a) The 3D model used for generating synthetic data shows the high resistive salt basement with uplifts, the reservoir, and the towline. (b) A 2D slice along the towline of the 3D resistivity model.

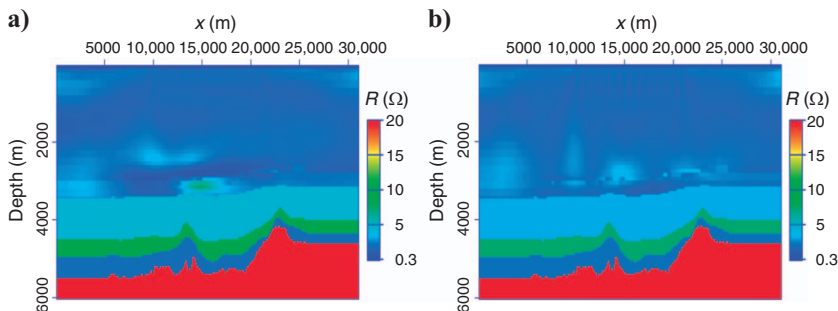**a)**   **b)**

Figure 4. (a) The inverted model after adding the frequency-differenced field into the misfit function, in addition to the conventional inline electric field. (b) The inverted model using only the conventional inline electric field.

CONCLUSION

By using frequency differencing, we have found that a significant improvement in depth penetration and resolution can be achieved. This is particularly true in a shallow-water environment. The method shows applicability at burial depths beyond what has previously been published. It is required to have a sufficiently high signal-to-noise ratio. However, this limitation is not more stringent than what is inherent in analyzing the signal-to-noise ratio for the single-frequency scattered field and is within reach of current acquisition technology. We believe that the presented method will significantly enhance the

potential for marine hydrocarbon surveying in shallow waters with CSEM.

REFERENCES

Abubakar, A., T. M. Habashy, V. L. Druskin, L. Knizhnerman, and D. Alumbaugh, 2008, 2.5D forward and inverse modeling for interpreting low-frequency electromagnetic measurements: Geophysics, **73**, no. 4, F165–F177.

Amundsen, L., L. O. Løseth, R. Mittet, S. Ellingsrud, and B. Ursin, 2006, Decomposition of electromagnetic fields into upgoing and downgoing components: Geophysics, **71**, no. 5, G211–G223.

Andreis, D., and L. MacGregor, 2008, Controlled-source electromagnetic sounding in shallow water: Principles and applications: Geophysics, **73**, no. 1, F21–F32.

Chave, A. D., and C. S. Cox, 1982, Controlled electromagnetic sources for measuring electrical conductivity beneath the oceans, 1. Forward problem and model study: Journal of Geophysical Research, **87**, 5327–5338.

Chen, J., and D. Alumbaugh, 2009, Three methods for mitigating airwaves in shallow water marine CSEM data: 79th Annual International Meeting, SEG, Expanded Abstracts, 785–789.

Commer, M., and G. A. Newman, 2008, New advances in three-dimensional controlled-source electromagnetic inversion: Geophysical Journal International, **172**, 513–535.

Constable, S., and L. J. Srnka, 2007, An introduction to marine controlled-source electromagnetic methods for hydrocarbon exploration: Geophysics, **72**, no. 2, WA3–WA12.

Eidesmo, T., S. Ellingsrud, L. M. MacGregor, S. Constable, M. C. Sinha, S. Johansen, F. N. Kong, and H. Westerdahl, 2002, Sea bed logging (SBL), a new method for remote and direct identification of hydrocarbon filled layers in deepwater areas: First Break, **20**, 144–152.

Ellingsrud, S., T. Eidesmo, S. Johansen, M. C. Sinha, L. M. MacGregor, and S. Constable, 2002, Remote sensing of hydrocarbon layers by seabed logging (SBL): Results from a cruise offshore Angola: The Leading Edge, **21**, no. 10, 972–982.

Hansen, K. R., and R. Mittet, 2009, Incorporating seismic horizons in inversion of CSEM data: 79th Annual International Meeting, SEG, Expanded Abstracts, 694–698.

Løseth, L. O., and L. Amundsen, 2007, Removal of air-responses by weighting inline and broadside CSEM/SBL data: 77th Annual International Meeting, SEG, Expanded Abstracts, 529–533.

Maaø, F. A., 2007, Fast finite-difference time-domain modeling for marine subsurface electromagnetic problems: Geophysics, **72**, no. 2, A19–A23.

MacGregor, L. M., and M. C. Sinha, 2000, Use of marine controlled source electromagnetic sounding for sub-basalt exploration: Geophysical Prospecting, **48**, 1091–1106.

Mittet, R., 2008, Normalized amplitude ratios for frequency-domain CSEM in very shallow water: First Break, **26**, 47–54.

Plessix, R. E., and W. A. Mulder, 2008, Resistivity imaging with controlled-source electromagnetic data: Depth and data weighting: Inverse Problems, **24**, 034012.

van den Berg, P. M., A. Abubakar, and T. M. Habashy, 2008, Removal of sea-surface-related wavefields and source replacement in CSEM data: 78th Annual International Meeting, SEG Expanded Abstracts, 672–676.

Weiss, C., 2007, The fallacy of the "shallow-water problem" in marine CSEM exploration: Geophysics, **72**, no. 6, A93–A97.